Synthesis, crystal structure characterization, DFT calculations, Hirshfeld surface analysis and 3D energy frameworks of triazole pyridazine derivatives: Theoretical and experimental studies

Hamdi Hamid Sallam [a,b], Yasser Hussien Issa Mohammed [c,d], Fares Hezam Al-Ostoot [c,e], Sridhar M. A. [a,*], Shaukath Ara Khanum [c]

[a] Department of Studies in Physics, Manasagangotri, University of Mysore, Mysuru 570 006, India
[b] Department of Physics, Faculty of Education and Science, Turba Branch, Taiz University, Yemen
[c] Department of Chemistry, Yuvaraja's College, University of Mysore, Mysuru 570 006, India
[d] Department of Biochemistry, Faculty of Applied Science, University of Hajjah, Yemen
[e] Department of Biochemistry, Faculty of Education and Science, Al-Baydha University, Yemen

ARTICLE INFO

ABSTRACT

Recently, pyridazine derivatives have shown considerable biological properties such as anti-tumor and anti-inflammatory activity. The studied compounds 6-chloro-3-[(4-methylphenoxy)methyl][1,2,4] triazolo[4,3-b]pyridazine (8a) and 6-chloro-3-[(4-fluorophenoxy)methyl][1,2,4] triazolo[4,3-b]pyridazine (8b) have been synthesized and characterized by NMR, IR and mass spectral studies, and finally, the structures were confirmed by single crystal X-ray diffraction technique. The compounds 8a and 8b have crystallized in the same crystal system with different space groups. Density functional theory calculations were performed to compare the theoretical and experimental results obtained from XRD. Further, DFT calculations were employed to determine HOMO-LUMO energy levels, energy gap, softness, hardness, and other quantum chemical parameters of the compounds 8a and 8b. Hirshfeld surface analysis was carried out to distinguish the different intermolecular hydrogen bonds. Energy frameworks for the compounds were constructed through different intermolecular interaction energies to know the dominant interaction energy involved in the molecular packing strength.

© 2021 Published by Elsevier B.V.

1. Introduction

In order to develop and produce new drugs that are effective against many diseases, especially those that occur in developing countries, research has often been focused on heteroatomic compounds [1–5]. In recent years, many researchers have been working on a variety of applications for aromatic heterocyclic derivatives, ranging from pharmaceuticals to synthetic uses [6–10]. Compounds with heteroaromatic scaffolds bearing one or more nitrogen atoms, such pyridazine, and its derivatives, have been important in medicinal chemistry and in many drug discovery programs [11–13]. The nitrogen-containing heterocycle pyridazine and its derivatives have been the focus of attention because of its easy functionalization at various ring positions making them attractive synthetic compounds for the design and development of

novel drugs of the future [14]. Pyridazine, as a "wonder nucleus", and its derivatives have been reported for their chemical and biological actions to possess a wide range of biological activities, including vasorelaxants, antihypertensive and potent cardiotonic agents [15–17], as well as their, anti-tuberculosis, anti-convulsant [18–20] anti-microbial and anti-inflammatory activities [21,22]. Various pyridazine based heterocyclic scaffolds have been utilized in recent medicinal chemistry programs against a range of biological targets and with various physiological effects and have found use as potent anti-cancer, anti-viral, analgesic, and anti-diabetic agents [23–26]. The pyridazine ring is a part of the structure of some therapeutic agents available in the market, including cadralazine, minaprine, hydralazine, and pipofezine [27–30]. As a result, there is continuing interest in the construction of new pyridazine compounds. Based on the broad biological activities of pyridazine [31] and also our ongoing research on the synthesis and characterization of heterocyclic derivatives, [32–34] the present article reports on the design, synthesis, and characterization of two new pyridazine derivatives. The compounds were characterised by various spectroscopic tech-

* Correspondence author at: Department of Studies in Physics, Manasagangotri, University of Mysore, Mysuru 570 006, India.
E-mail addresses: hamdisallam2014@gmail.com (H.H. Sallam), mas@physics.uni-mysore.ac.in (S. M. A.).
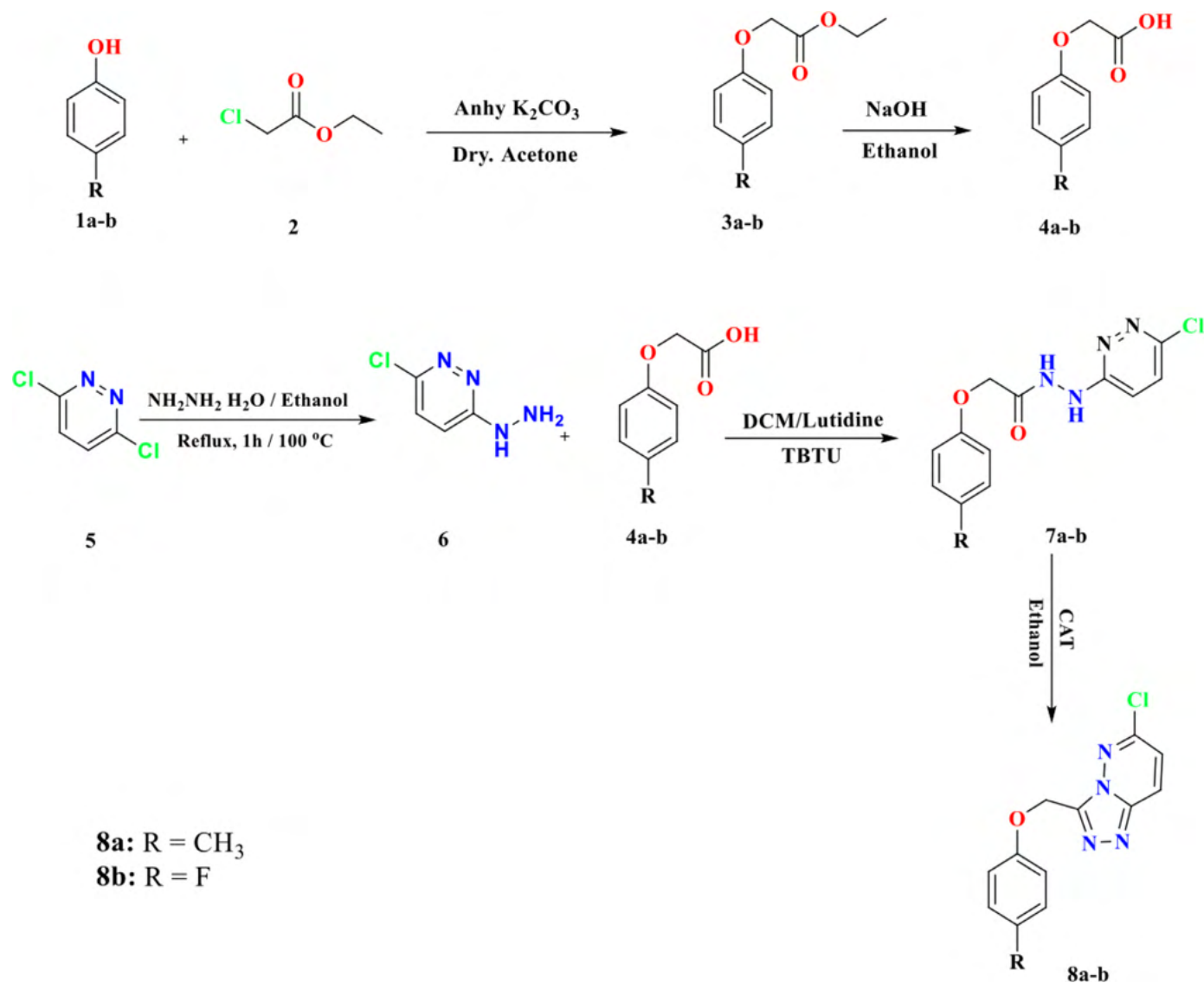
Fig. 1. Reaction pathway for the synthesis of the title compounds (8a-b).

niques and the structures were determined by a single crystal X-ray structural analysis. In the present study, we report the theoretical and experimental results of the compounds 6-chloro-3-[(4-methylphenoxy)methyl][1,2,4]triazolo[4,3-b]pyridazine and 6-chloro-3-[(4-fluorophenoxy)methyl][1,2,4]triazolo[4,3-b]pyridazine by employing Density Functional Theory (DFT), Hirshfeld surface analysis, and energy frameworks calculations.

2. Experimental details

2.1. Materials and methods

The chemicals required for the synthesis of title compounds (8a-b) were procured from Sigma Aldrich Chemical Co. The progress of the reaction was monitored by Thin Layer Chromatography (TLC) preformed on aluminum-backed silica plates, and the spots were detected by exposure to UV-lamp at $\lambda = 254$ nm. Melting point and boiling point were measured on a Chemiline, microcontroller based melting point/boiling point-Cl725 apparatus with a digital thermometer. IR spectra were recorded on the Agilent Technologies Cary 630 FTIR spectrometer. ^{1}H and ^{13}C NMR spectra were recorded on VNMRS-400 Agilent-NMR spectrophotometer.

The mass spectra were obtained with a VG70-70H spectrometer. The elemental analysis (C, H, and N) was performed on Elementar Vario EL III elemental analyzer. The result of elemental analysis is within $\pm 0.4\%$ of the theoretical value. More experimental details and the ^{1}HNMR spectra of the two compounds are given in the supplementary file (Figures S1 and S2). The schematic diagram of the synthesized compounds is shown in Fig. 1.

2.2. Crystallographic data collection, structure solution and refinement

A block of yellow colored single crystal of 8a and a colorless single crystal of 8b with approximate dimensions $0.20 \times 0.15 \times 0.10$ mm^3 were chosen for X-ray data collection. The data were collected on a Bruker CMOS diffractometer equipped with MoK$_\alpha$ radiation with wavelength 0.71073 Å [35] at 293 K. The intensity data reduction was done using SAINT PLUS [36] software package. Data were corrected for absorption effects using the multi-scan method. The crystal structure was solved by the direct method using SHELXS-97 and the refinement against F^2 was carried out using SHELXL-97 [37]. All the non-hydrogen atoms were refined anisotropically. Hydrogen atoms attached to carbon atoms

Table 1
The crystal data and structure refinement details.

Parameter	Compound 8a	Compound 8b
CCDC deposit No.	1838281	1839207
Empirical formula	$C_{13}H_{11}ClN_4O$	$C_{12}H_8ClFN_4O$
Formula weight	274.71	278.67
Temperature	293(2) K	293(2) K
Radiation, Wavelength	MoK_α, 0.71073 Å	MoK_α, 0.71073 Å
θ range for entire data collection	3.00º to 26.40º	3.20º to 27.22º
Crystal system, Space group	Monoclinic, $P2_1/c$	Monoclinic, $P2_1$
Cell parameters	a = 12.0965(7) Å	a = 8.2431(4) Å
	b = 13.6075(7) Å	b = 6.0342(3) Å
	c = 7.7686(4) Å	c = 12.5424(7) Å
	β = 93.942(3)º	β = 99.092(2)º
Volume	1275.71(12) Å³	616.03(5) Å³
Z	4	2
Density (calculated)	1.430 Mg m⁻³	1.502 Mg m⁻³
Absorption coefficient	0.296 mm⁻¹	0.319 mm⁻¹
F_{000}	568	284
Index ranges	$-15 \leq h \leq 15$	$-11 \leq h \leq 11$
	$-17 \leq k \leq 17$	$-8 \leq k \leq 8$
	$-9 \leq l \leq 9$	$-17 \leq l \leq 17$
Reflections collected	38427	16227
Independent reflections	2606 [R_{int} = 0.0569]	3621 [R_{int} = 0.0304]
Absorption correction	Multi-scan	Multi-scan
Refinement method	Full matrix least-squares on F^2	Full matrix least-squares on F^2
Data / restraints / parameters	2606 / 0 / 174	3621 / 1 / 172
Goodness-of-fit on F^2	1.110	1.018
Final [I > 2σ(I)]	R1 = 0.0530, wR₂ = 0.1416	R1 = 0.0412, wR₂ = 0.0844
R indices (all data)	R1 = 0.0782, wR₂ = 0.1686	R1 = 0.0689, wR₂ = 0.0941
Largest diff. peak and hole	0.345 and −0.322 eÅ⁻³	0.156 and − 0.159 e Å⁻³

were allowed to ride on their parent atoms. Using PLATON [38], geometrical calculations were carried out and the ORTEP and molecular figures were generated using MERCURY [39]. For 8a, a total of 174 parameters were refined with 2606 unique reflections, whereas for 8b, a total of 172 parameters were refined with 3621 unique reflections. The residual factor of 8a and 8b are 0.0530 and 0.0412 respectively. Crystallographic data (CIF) of the compounds 8a and 8b has been deposited at the Cambridge Crystallographic Data Centre with CCDC numbers: 1838281 and 1839207 respectively.

3. Computational studies

The density functional theory (DFT) calculations for the compounds 8a and 8b were performed using Gaussian 09 software [40]. They were carried out with Becke three parameter for the exchange with correlation functional of Lee-Yang-Parr (B3LYP) for 6-31+G(d,p) basis sets. The Hirshfeld surface analysis, 2D fingerprint, and energy frameworks calculations for the title compounds have been studied by using CrystalExplorer-17 program [41].

4. Structural characterisation

4.1. X-ray diffraction and DFT calculations

The 3D structure of the compounds was confirmed by single crystal X-ray diffraction studies. The compounds 8a and 8b crystallize in the monoclinic crystal system with the space group $P2_1/c$ and $P2_1$ respectively. The crystal data and refinement details of the title compounds are tabulated in Table 1. The density functional theory (DFT) calculations were adopted for geometry optimization. DFT calculations depend on the electron density distribution function of the studied compound. The ORTEP diagram and calculated optimized structure of the title compounds are shown in Fig. 2. The comparison between experimental and theoretical results of selected, bond lengths, bond angles, and torsion angles are listed in Tables 2–4 respectively. The values of bond lengths and bond angles obtained by DFT, and the XRD analysis are plotted (the full

Table 2
Comparison of bond lengths of selected non-hydrogen atoms.

Compound 8a			Compound 8b		
Atoms	Bond lengths (Å)		Atoms	Bond lengths (Å)	
	XRD	DFT		XRD	DFT
C1-C2	1.509(4)	1.5126	F1-C2	1.374(3)	1.3941
C3-C4	1.381(3)	1.3906	C3-C4	1.384(3)	1.3933
O8-C9	1.412(2)	1.4087	O8-C9	1.426(2)	1.4604
C9-C10	1.483(3)	1.4978	C9-C10	1.475(3)	1.4783
N12-C13	1.311(3)	1.3234	N12-C13	1.313(2)	1.3397
Cl19-C16	1.722(2)	1.7446	Cl19-C16	1.724(2)	1.8051

Table 3
Comparison bond angles of selected non-hydrogen atoms.

Compound 8a			Compound 8b		
Atoms	Bond angles (°)		Atoms	Bond angles (°)	
	XRD	DFT		XRD	DFT
C1-C2-C3	121.0(2)	120.99	F1-C2-C3	118.1(2)	118.82
C4-C5-C6	119.5(2)	119.72	C4-C5-C6	120.1(2)	120.50
O8-C9-C10	107.9(2)	108.47	O8-C9-C10	107.1(1)	107.31
N12-C13-C18	134.2(2)	133.65	N12-C13-C18	133.3(2)	133.36
N15-C16-C17	126.6(2)	125.82	N15-C16-C17	126.5(2)	126.23
Cl19-C16-N15	114.7(2)	115.87	Cl19-C16-N15	115.4(1)	115.72

lists are given in Tables S1 and S2 of the supplementary file) as shown in Figure S3 of supplementary file. This Figure illustrates the agreement between DFT and XRD bond lengths with correlation coefficient R^2 = 0.9828 and 0.9784 for 8a and 8b respectively. Agreement is noticeable between DFT and XRD bonds angles with R^2 = 0.9902 and 0.9945 for 8a and 8b respectively and these results show a good agreement between theoretical and experimental values for the compounds.
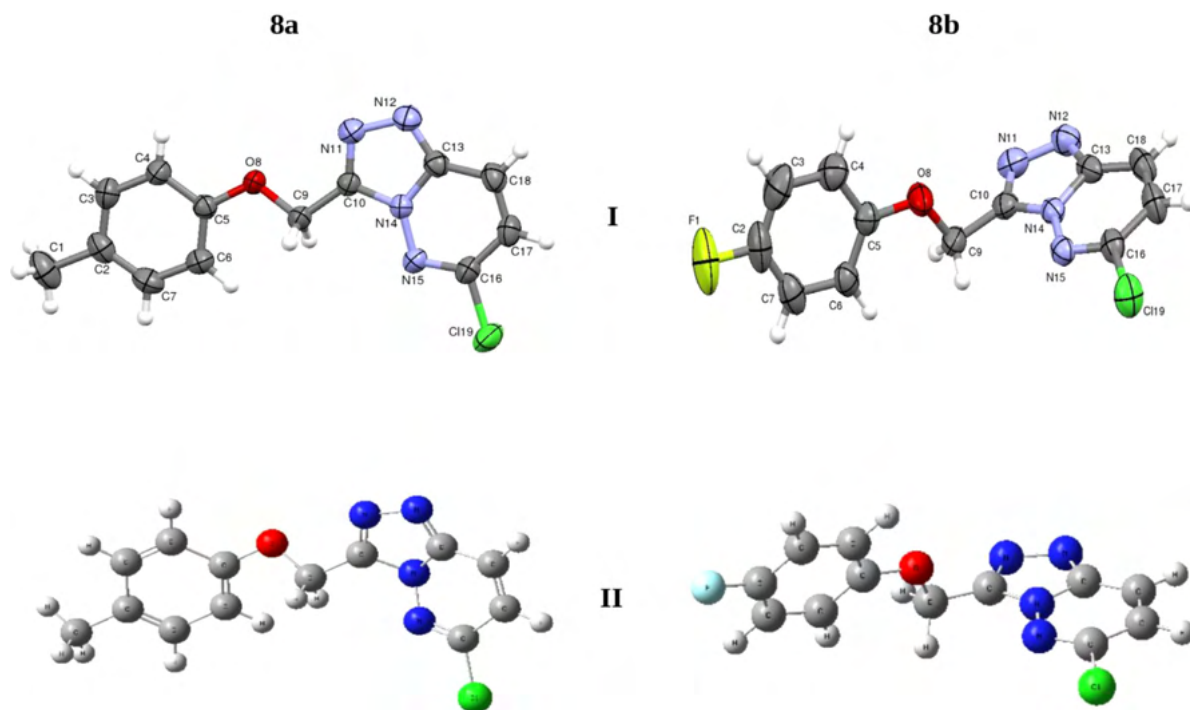
Fig. 2. Molecular structures of the molecules 8a and 8b: I) The thermal ellipsoid plot of the compounds with 50% probability ellipsoids and II) Optimized structures of the compounds.

Table 4
Comparison torsion angles of selected non-hydrogen atoms.

Compound 8a			Compound 8b		
Atoms	Torsion angles (°)		Atoms	Ttorsion angles (°)	
	XRD	DFT		XRD	DFT
C1-C2-C3-C4	−179.4(2)	-178.89	F1-C2-C3-C4	178.9(2)	179.92
C3-C2-C7-C6	−0.2(4)	-0.21	C3-C2-C7-C6	0.4(4)	0.03
C5-O8-C9-C10	178.8(2)	-179.03	C5-O8-C9-C10	169.5(1)	-177.07
C10-N14-C13-N12	0.0(2)	-0.01	C10-N14-C13-N12	−0.7(2)	-0.38
C13-N14-C10-N11	−0.2(2)	-0.02	C13-N14-C10-N11	0.4(3)	0.21
Cl19-C16-C17-C18	179.2(2)	-179.98	Cl19-C16-C17-C18	178.3(1)	179.22

4.2. Frontier molecular orbitals and global reactivity descriptors

The frontier molecular orbitals HOMO (highest occupied molecular orbital) and LUMO (lowest unoccupied molecular orbital) of compounds 8a and 8b were generated. Those orbitals are responsible for the kinetic energy and chemical reactivity of the compound where the energy gap between the molecular orbitals describes the chemical stability and reactivity of the molecule. If the orbital energy gap of the molecule is small that refers to a soft molecule and high chemical reactivity while a large value of orbital energy gap is associated with the low chemical reactivity and refers to hard molecule [42,43]. The molecular orbitals HOMO and LUMO with the energy gap for the compounds are shown in Fig. 3. The estimated energy gap (ΔE) between the HOMO (E_H) and LUMO (E_L) energies levels of compounds 8a and 8b are 3.252 eV and 3.474 eV respectively, which implies that the molecules are soft, unstable, and reactive. The lower energy gap explains the easy transfer of electrons taking place within the molecule [44,45]. For 8a and 8b, HOMO occurs in the phenoxy ring, oxygen atom, and methylene, while the LUMO is localized in the triazole, pyridazine rings, and chlorine atom.

The global chemical reactivity descriptors enable us to know the chemical properties of the compound. Ionization potential (I)

is a measure of electron donating power of a molecule which is given as I = $-E_H$. The electron affinity (A) characterizes the ability of a molecule to accept electrons and it is calculated by A = $-E_L$. The difference between (E_H) and (E_L) is the energy gap (ΔE), which determines the hardness, softness and chemical reactivity of the molecule. The chemical hardness (η) is one-half of the energy gap i.e., $\eta = \Delta E/2$, while global softness (σ) of the molecule is calculated by the formula $\sigma = 1/2\eta$. Electronegativity (χ) is the tendency of an atom in a molecule to attract shared electrons and it is given by $\chi = (I+A)/2$. Chemical potential (μ) of the molecule is expressed as $\mu = -\chi$. Eletrophilicity (ω) specifies the electrophilic power of a molecule and is calculated by $\omega = \mu^2/2\eta$. Table 5 summarizes the calculated energies of different FMOs, energy gap, and the molecular reactivity descriptors for 8a and 8b.

4.3. Description of the structures

All the rings in the structures are planar. The maximum deviation from the plane for the pyridazine ring (C13-N14-N15-C16-C17-C18) in 8a and 8b are -0.011(2) Å and 0.011(2) Å for C18 and C16 respectively. The maximum deviation from the plane for the triazole ring (C10-N11-N12-C13-N14) in 8a and 8b are 0.002(2) Å and 0.004(2) Å for N11 and C13 respectively; for the 9 mem-
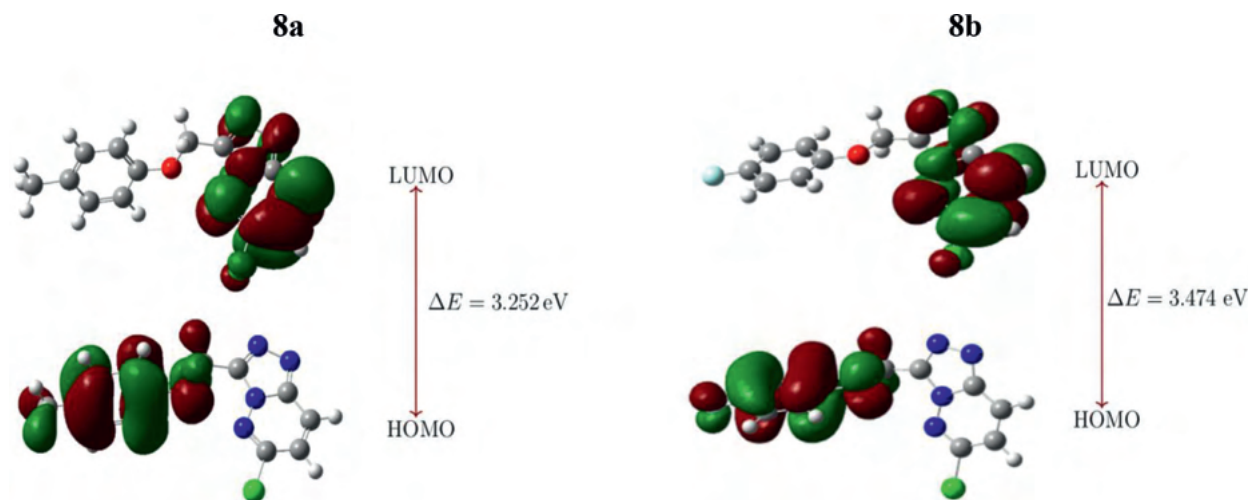
Fig. 3. HOMO-LUMO energy levels and energy gap of the compounds.

Table 5
Calculated energy values and quantum molecular descriptors of compounds 8a and 8b.

Parameters	Symbol and formula	8a	8b
HOMO energy	E_H (eV)	-5.905	-6.237
LUMO energy	E_L (eV)	-2.653	-2.763
Energy gap	$\Delta E = E_H - E_L$ (eV)	3.252	3.474
Ionization potential	$I = -E_H$ (eV)	5.905	6.237
Electron affinity	$A = -E_L$ (eV)	2.653	2.763
Chemical hardness	$\eta = \Delta E/2$ (eV)	1.626	1.736
Global softness	$\sigma = 1/2\eta$ (eV^{-1})	0.307	0.287
Eletronegativity	$\chi = (I + A)/2$ (eV)	4.279	4.500
Chemical potential	$\mu = -\chi$ (eV)	-4.279	-4.500
Eletrophilicity	$\omega = \mu^2/2\eta$ (eV)	5.630	5.830

bered ring (C10-N11-N12-C13-C18-C17-C16-N15-N14) in 8a and 8b are 0.019(2) Å and 0.022(2) Å for C17 and C16 respectively. The maximum deviation from the plane for the phenoxy ring (C2-C3-C4-C5-C6-C7) in 8a and 8b are 0.004(2) Å and 0.002(3) Å for C3 and C2-C3-C4 fragment, respectively.

The methoxy-phenoxy ring in compound 8a is in plane with the fused triazole-pyridazine ring system as indicated by the torsion angle values of 178.8(2)° for the atoms bridge C5-O8-C9-C10. The fluoro-phenoxy ring in compound 8b is almost perpendicular to the fused triazole-pyridazine ring system, the dihedral angle between the two rings is 75.13(6)°. The triazole and fluoro-phenoxy rings are bridged by C5-O8-C9-C10 atoms with torsion angle = 169.5(2)°. In compound 8a, the effect of the methyl group shows distortion in the ring yielding an angle smaller than the typical hexagonal (120°) at the position of substitution i.e., C3-C2-C7 = 117.0(2)°. This effect is in reverse with a fluorine atom in compound 8b that exhibits an angle greater than 120° at the position of substitution i.e., C3-C2-C7 = 123.2(3)°.

In 8a molecules are connected by intermolecular hydrogen bonds (given in Table 6) to form a layer parallel with the bc plane. The molecules of 8b are connected by hydrogen bonds (given in Table 7) into chains running parallel with the b crystallographic axis. The packing of the molecules for each compound is shown in Fig. 4. Additionally, 8a structure reinforced by medium to weak π-π interactions, as the centroid-centroid distance between the rings is less than 3.8Å whereas, in 8b structure there are two C16-Cl19...Cg interactions. π-π interactions of 8a and C–Cl···Cg of 8b are given in the supplementary file as Tables S3 and S4 respectively.

4.4. Hirshfeld surface analysis and 2D fingerprint plots

Hirshfeld surface is a unique method for realising the intermolecular interactions and obtaining information on trends in crystal packing [46]. The mapping of Hirshfeld surface over the normalized contact distance d_{norm} was carried out for the compounds 8a and 8b as illustrated in Fig. 5. This mapping shows red, blue, and white color schemes. The red (d_{norm} is negative) and blue (d_{norm} is positive) colored regions on the surface are from shorter and longer contacts than van der Waals radii respectively; while the white colored regions represent the contacts that are equal to the van der Waals radii or $d_{norm} = 0$ [47]. The bright red region in 8a marked as 1 is from C9-H9B...O8 contact, 2 and 3 are from C17-H17...N11 intermolecular hydrogen bonds, whereas in 8b the bright red region marked as 1 is from C9–H9B...N12 contact, 2 and 3 are from C9–H9A...F1 intermolecular hydrogen bonds. Hirshfeld surface volumes of 8a and 8b are 312.06 Å^3 and 301.47 Å^3 respectively.

The 2D fingerprint plots were generated to know the percentage of the intermolecular contributions of intermolecular interactions of each type of contact to the total Hirshfeld surface area [48]. Fig. 6a shows the 2D fingerprint of all the contacts. The major contribution of 8a is from H-H contacts (28.2%), while the major contribution of 8b is from C-H contacts (19.0%) to the total Hirshfeld surface area (Fig. 6b). The remaining contributions of 8a are from N-H, Cl-H, C-H, O-H contacts, which contribute about 20.2%, 19.0%, 13.5%, 5.2% respectively to the Hirshfeld surface area. The remaining contributions of 8b are from N-H, F-H, H-H, Cl-H, O-H contacts, which contribute about 17.3%, 14.7%, 13.8%, 10.7%, 4.6% respectively to the total Hirshfeld surface area. The strong intermolecular interactions appear as distinct spikes in the fingerprint plots. N-H interactions appear as two characteristic spikes which have a significant contribution to the crystal packing of 8a and 8b where the distance $d_i + d_e \approx 2.5$ Å (Fig. 6c). Furthermore, O-H and F-H interactions appear as two characteristic spikes with a significant contribution to the crystal packing for 8a and 8b respectively, where the distance $d_i + d_e \approx 2.35$ Å and 2.4 Å (Fig. 6d).

4.5. 3D Energy frameworks analysis

The study of energy frameworks gives insight into the unique quantitative analysis of interaction energies and supramolecular architecture of molecules in the crystal. A cluster of molecules within a radius of 3.8 Å was generated around a single molecule of 8a and 8b. The scale factors used for the construction of the energy frame-

Table 6
Hydrogen bonds geometry 8a.

D-H... A	D-H (Å)	H ... A (Å)	D ... A (Å)	D-H ... A (°)	Symmetry codes
C9–H9B...O8	0.97	2.50	3.439(3)	164	x, 1/2-y, 1/2+z
C17–H17...N11	0.93	2.56	3.260(3)	132	1-x, 1/2+y, -1/2-z

Table 7
Hydrogen bonds geometry of 8b.

D-H... A	D-H (Å)	H... A (Å)	D... A (Å)	D-H... A (°)	Symmetry codes
C9–H9A...F1	0.97	2.52	3.449(3)	160	3-x, -1/2+y, 2-z
C9–H9B...N12	0.97	2.59	3.418(3)	143	x, 1+y, z
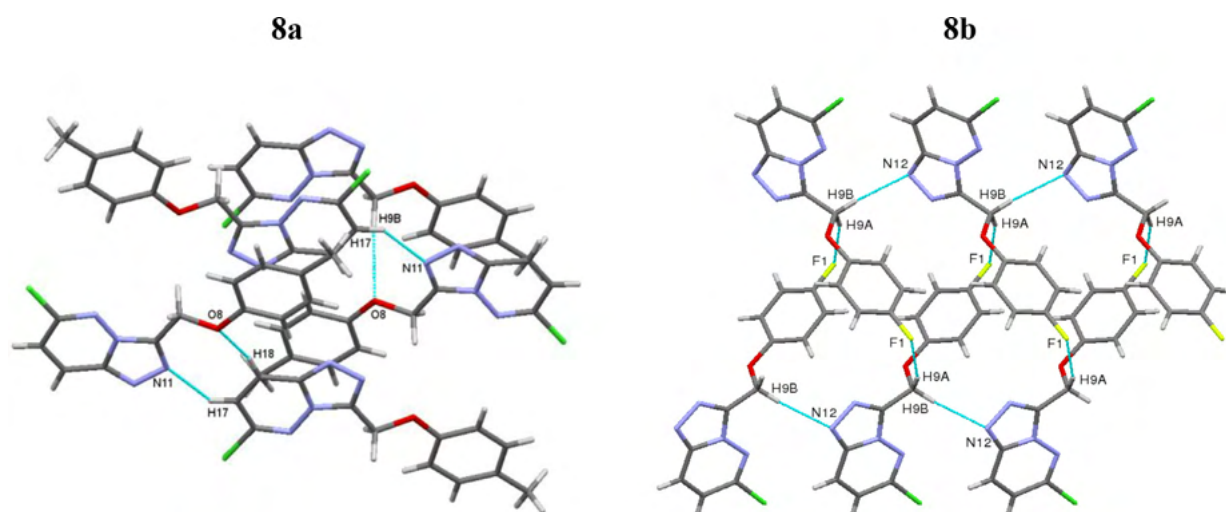
Fig. 4. The packing of the molecules for the title compounds.
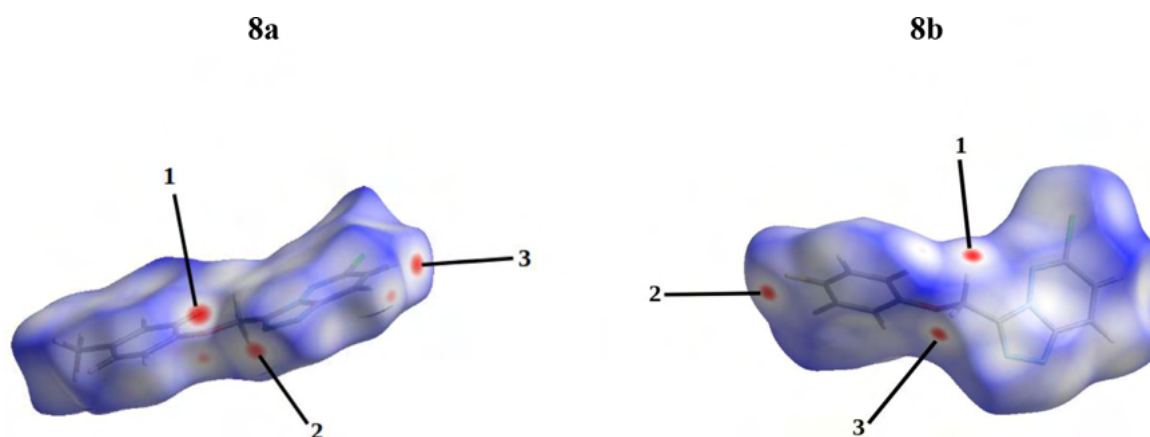
Fig. 5. Hirshfeld surface mapped over d_{norm}.

work for B3LYP/6-31G (d,p) electron densities are k_ele = 1.057, k_pol = 0.740, k_disp = 0.871, k_rep = 0.618 [49]. Table 8 lists the calculated interaction energies in kJ/mol and the symmetry operations for nine molecules of 8a. The red colored molecule located at 4.56 Å from the centroid of the selected molecule showing the highest total interaction energy (-46.5 kJ/mol) whereas the green colored molecule at 11.88 Å from the centroid of the selected molecule exhibits the lowest total interaction energy (-2.9 kJ/mol). Table 9 lists the calculated interaction energies in kJ/mol and the symmetry operations for seven molecules of 8b. The red colored molecule at 6.03 Å from the centroid of the selected molecule showing the highest total interaction energy (-33.8

kJ/mol) whereas the turquoise colored molecule located at 12.54 Å from the centroid of the selected molecule exhibits the lowest total interaction energy (-3.1 kJ/mol). Molecular pairs involved in the calculation of interaction energies of 8a and 8b along the b axis are shown in Fig. 7. The Coulomb interactions in 8a, look to be more in strength than in 8b as R values (the mean atomic distance between molecular centroids in Å) of 8a are smaller than the values of 8b. The calculated interaction energies for electrostatic, polarization, dispersion, and repulsion of 8a are -71.3 kJ/mol, -23.6 kJ/ mol, -194.0 kJ/mol, and 117.0 kJ/mol respectively. The calculated interaction energies for electrostatic, polarization, dispersion, and repulsion of 8b are -58.4 kJ/mol, -15.0 kJ/ mol, -134.0
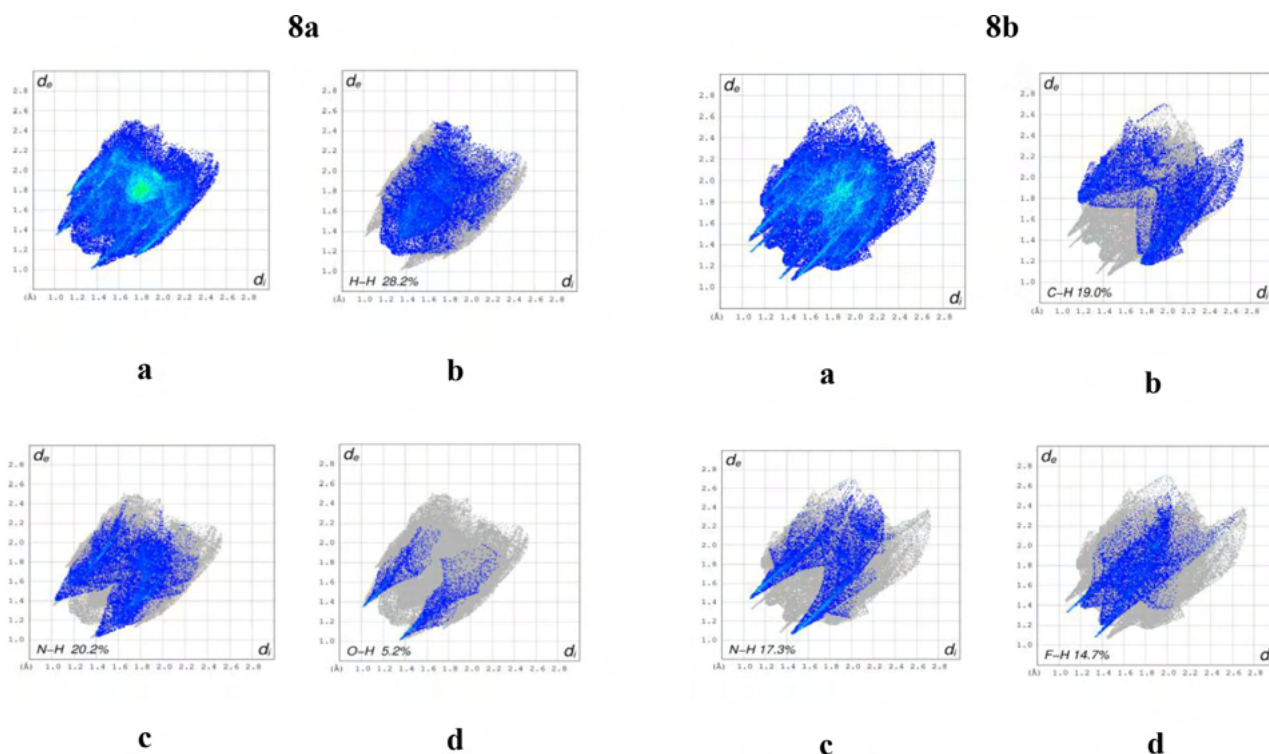
8a

8b

Fig. 6. 2D fingerprint plots of 8a and 8b (a) From all the contacts and (b-d) Decomposed fingerprint plot showing contacts for specific pairs of atoms.
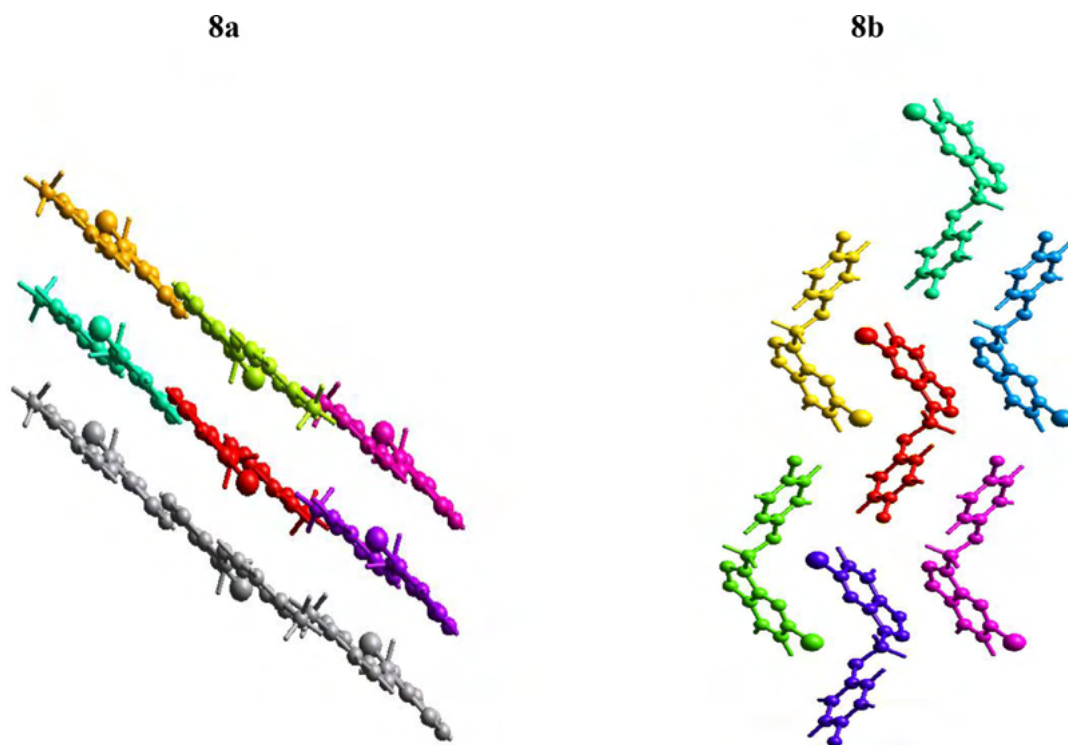
8a

8b

Fig. 7. Molecular pairs involved in the calculation of interaction energies of 8a and 8b along b axis

kJ/mol, and 88.2 kJ/mol respectively. The total energies of 8a and 8b are -189.1 kJ/mol and -135.0 kJ/mol respectively. It is clear that the dispersion energy has the highest value among all interaction energies in 8a and 8b i.e., the dispersion interaction energy dominates over the electrostatic Coulomb interaction energy. This is because of the presence of chloro group which has a large electron cloud in each compound. The more electrons an atom or molecule

has, the stronger dispersion forces are. The scale factors for benchmarked energies used for the construction of energy models were taken from Mackenzie et al. [50]. The visualization of different interaction energies like Coulomb interaction energy, dispersion energy, total interaction energy are represented by red, green, and blue color respectively for the compounds 8a and 8b along different axes are shown in Fig. 8. The cylinders in the energy frame-

Table 8
Different interaction energies of the molecular pairs in kJ/mol of 8a.

N	Symmetry operation	R (Å)	Electron density	E_ele	E_pol	E_dis	E_rep	E_tot
2	x, -y+1/2, z+1/2	4.56	B3LYP/6-31G(d,p)	-13.6	-5.0	-59.6	37.9	-46.5
2	-x, y+1/2, -z+1/2	9.29	B3LYP/6-31G(d,p)	-28.2	-8.4	-19.6	21.5	-39.9
2	x, y, z	13.61	B3LYP/6-31G(d,p)	-2.1	-0.2	-6.0	5.3	-4.2
2	x, -y+1/2, z+1/2	11.88	B3LYP/6-31G(d,p)	1.1	-0.6	-7.0	4.0	-2.9
1	-x, -y, -z	6.98	B3LYP/6-31G(d,p)	-3.7	-4.5	-44.7	20.1	-33.7
1	-x, -y, -z	10.04	B3LYP/6-31G(d,p)	-18.2	-3.3	-9.0	3.6	-27.2
1	-x, -y, -z	11.37	B3LYP/6-31G(d,p)	-3.6	-1.1	-27.3	14.3	-19.5
1	-x, -y, -z	13.60	B3LYP/6-31G(d,p)	-0.6	-0.1	-7.8	2.6	-5.9
2	-x, y+1/2, -z+1/2	10.20	B3LYP/6-31G(d,p)	-2.4	-0.4	-13.0	7.7	-9.3

Table 9
Different interaction energies of the molecular pairs in kJ/mol of 8b.

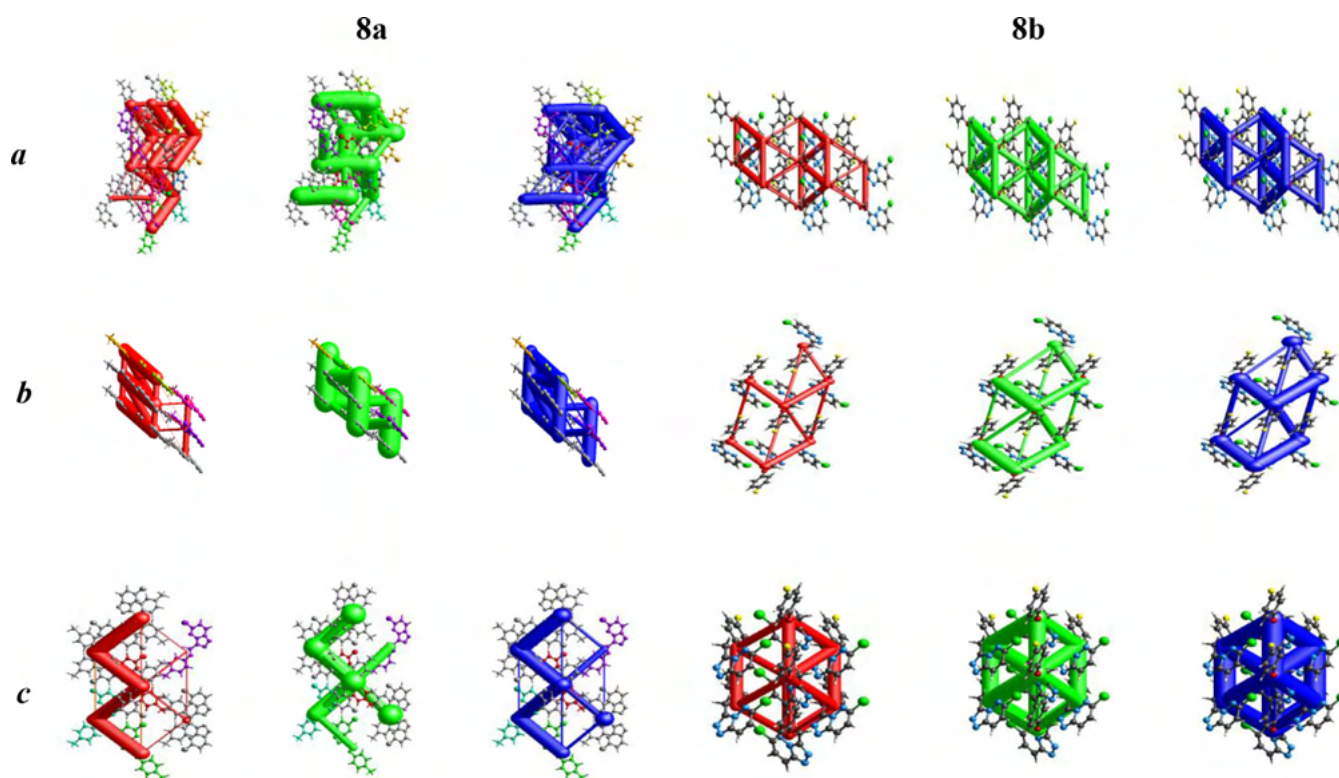| N	Symmetry operation	R (Å)	Electron Density	E_ele	E_pol	E_dis	E_rep	E_tot
2	x, y, z	6.03	B3LYP/6-31G(d, p)	-17.8	-4.9	-31.2	25.5	-33.8
2	-x, y+1/2, -z	6.13	B3LYP/6-31G(d, p)	-12.3	-1.9	-35.3	24.0	-30.4
2	-x, y+1/2, -z	10.19	B3LYP/6-31G(d, p)	-0.7	-0.3	-9.8	3.8	-7.2
2	x, y, z	12.54	B3LYP/6-31G(d, p)	-0.6	-0.2	-3.9	1.6	-3.1
2	-x, y+1/2, -z	7.16	B3LYP/6-31G(d, p)	-16.2	-5.5	-27.7	18.5	-33.9
2	x, y, z	13.92	B3LYP/6-31G(d, p)	-4.7	-1.0	-6.3	3.6	-9.0
2	-x, y+1/2, -z	9.21	B3LYP/6-31G(d, p)	-6.1	-1.2	-19.8	11.2	-17.6

Fig. 8. The graphical representation of electrostatic interactions: Coulomb interaction energy (red), dispersion energy (green), and total interaction energy (blue) of 8a and 8b along a, b and c axes.

work represent the relative strengths of molecular packing in several directions. In order to contract or expand the size of the cylinders in the framework, an overall scale factor is used [51]. There is an absence of cylinders in a particular direction due to the exclusion of a few interactions under certain threshold energy. These weaker interactions have been ignored only to make the figures less crowded.

5. Conclusions

In summary, pyridazine derivatives (8a and 8b) were synthesized in excellent yield and characterized to confirm their struc-

tures. For these two compounds, the DFT geometries are in good agreement with XRD results. The low energy gap between the frontier molecular orbitals indicates soft and unstable molecules with easy transfer of electrons from HOMO to LUMO. The structures are stabilized by different hydrogen bond interactions. Hirshfeld surface studies reveal the types of intermolecular interactions of molecules and 2D fingerprint plots present the percentage of each type of contact for 8a and 8b. From energy 3D frameworks analysis, it is found out that dispersion energy is the dominant factor among all interaction energies, this is due to the presence of chloro group which has large electron cloud in the two compounds.

Credit author statement

All authors have contributed in preparation of the manuscript. Hamdi Hamid Sallam: Analysis and interpretation of the data, calculations, visualization, conceptualization, methodology, and writing-original draft of the manuscript. Yasser Hussien Issa Mohammed and Fares Hezam Al-Ostoot: Synthesis, spectroscopic characterizations and writing-original chemistry manuscript draft. Sridhar M. A.: Investigation, supervision, and approval of the final version of the manuscript. Shaukath Ara Khanum: Synthesis, and approval the chemistry manuscript draft.

Declaration of Competing Interest

The authors declare that they have no known competing financial interests or personal relationships that could have appeared to influence the work reported in this paper. This manuscript has not been submitted to, nor is under review at, another journal or other publishing venue. The authors have no affiliation with any organization with a direct or indirect financial interest in the subject matter discussed in the manuscript.

Acknowledgements

Supplementary materials

Supplementary material associated with this article can be found, in the online version, at doi:10.1016/j.molstruc.2021.131242.

References

[1] A. Gomtsyan, Heterocycles in drugs and drug discovery, Chem. Heterocycl. Compd. 48 (2012) 7–10.

[2] M. Baumann, I.R. Baxendale, An overview of the synthetic routes to the best selling drugs containing 6-membered heterocycles, Beilstein J. Org. Chem. 9 (2013) 2265–2319.

[3] J.A. Ayukekbong, M. Ntemgwa, A.N Atabe, The threat of antimicrobial resistance in developing countries: causes and control strategies, Antimicrob. Resistance Infect. Control 6 (2017) 47.

[4] F.H. Al-Ostoot, Y.H.E. Mohammed, A.N.Kempaiah. Zabiulla, S..A. Khanum, Synthesis, in silico study and in vitro anti-microbial evaluation of some new N-benzoyl- N'-[2-(4-chloro-phenoxy)-acetyl]-hydrazides analogs, J. Appl. Pharmaceut. Sci. 9 (2019) 042–049.

[5] R.J. Fair, Y. Tor, Antibiotics and bacterial resistance in the 21st century, Perspect. Med. Chem. 6 (2014) 25–64.

[6] A.P. Taylor, R.P. Robinson, Y.M. Fobian, D.C. Blakemore, L.H. Jones, O. Fadeyi, Modern advances in heterocyclic chemistry in drug discovery, Org. Biomol. Chem. 14 (2016) 6611–6637.

[7] A. Dastan, A. Kulkarni, B. Torok, Environmentally benign synthesis of heterocyclic compounds by combined microwave-assisted heterogeneous catalytic approaches, Green Chem. 14 (2012) 17–37.

[8] K. Kumara, F..H. Al-Ostoot, Y.H.E. Mohammed, S.A. Khanum, N.K. Lokanath, Synthesis, crystal structure and 3D energy frameworks of ethyl 2-[5-nitro-2-oxopyridine-1 (2H)-yl] acetate: Hirshfeld surface analysis and DFT calculations, Chem. Data Collect. 20 (2019) 100195.

[9] Y.H..E. Mohammed, V.H. Malojirao, P. Thirusangu, M. Al-Ghorbani, B.T. Prabhakar, S.A. Khanum, The Novel 4-Phenyl-2-Phenoxyacetamide Thiazoles modulates the tumor hypoxia leading to the crackdown of neoangiogenesis and evoking the cell death, Eur. J. Med. Chem. 143 (2018) 1826–1839.

[10] Q. Xu, Y. Wang, J. Xu, M. Sun, H. Tian, D. Zuo, Q. Guan, K. Bao, Y. Wu, W. Zhang, Synthesis and bioevaluation of 3, 6-diaryl-[1, 2, 4] triazolo [4, 3-b] pyridazines as antitubulin agents, ACS Med. Chem. Lett. 7 (2016) 1202–1206.

[11] Y.H.E. Mohammed, P. Thirusangu, V. Vigneshwaran, B.T. Prabhakar, S.A. Khanum, The anti-invasive role of novel synthesized pyridazine hydrazide appended phenoxy acetic acid against neoplastic development targeting matrix metallo proteases, Biomed. Pharmacother. 95 (2017) 375–386.

[12] H.B. Abed, O. Mammoliti, O. Bande, G.V. Lommen, P. Herdewijn, Strategy for the synthesis of pyridazine heterocycles and their derivatives, J. Org. Chem. 78 (2013) 7845–7858.

[13] R.M. Butnariu, I.I. Mangalagiu, New pyridazine derivatives: synthesis, chemistry and biological activity, Bioorg. Med. Chem. 17 (2009) 2823–2829.

[14] M. Asif, Diverse biologically active pyridazine analogs: a scaffold for the highly functionalized heterocyclic compounds, Rev. J. Chem. 8 (2018) 280–300.

[15] E.N. Amin, A.A..M. Abdel-Alim, S..G. Abdel-Moty, A.N.A. El-Shorbagi, M.S. Abdel-Rahman, Synthesis of new 4, 5-3 (2H) pyridazinone derivatives and their cardiotonic, hypotensive, and platelet aggregation inhibition activities, Arch. Pharm. Res. 33 (2010) 25–46.

[16] T. Wang, Y. Dong, L.C. Wang, B.R. Xiang, Z. Chen, L.B. Qu, Design, synthesis and structure-activity relationship studies of 6-phenyl-4, 5-dihydro-3 (2H)-pyridazinone derivatives as cardiotonic agents, Arzneimittelforschung 58 (2008) 569–573.

[17] E. Goessnitzer, A. Krbavcic, W. Wendelin, M. Krbavcic, Synthesis and Structure Investigations of Potential Sedative and Anticonvulsant Hydroxy-and Acetoxy-N-(3-oxobutyl)-pyrido [2, 3-d] pyridazinones, Monatshefte für Chemie/Chemical Monthly 133 (2002) 1177–1185.

[18] A.A. Siddiqui, R. Mishra, M. Shaharyar, A. Husain, M. Rashid, P. Pal, Triazole incorporated pyridazinones as a new class of antihypertensive agents: design, synthesis and in vivo screening, Bioorg. Med. Chem. Lett. 21 (2011) 1023–1026.

[19] D. Mantu, M.C. Luca, C. Moldoveanu, G. Zbancioc, I.I. Mangalagiu, Synthesis and antituberculosis activity of some new pyridazine derivatives. Part II, Eur. J. Med. Chem. 45 (2010) 5164–5168.

[20] B. Sharma, A. Verma, U.K. Sharma, S. Prajapati, Efficient synthesis, anticonvulsant and muscle relaxant activities of new 2-((5-amino-1, 3, 4-thiadiazol-2-yl) methyl)-6-phenyl-4, 5-dihydropyridazin-3 (2H)-one derivatives, Med. Chem. Res. 23 (2014) 146–157.

[21] R.M. Butnariu, M.D. Caprosu, V. Bejan, I.I. Mangalagiu, M. Ungureanu, A. Poiata, C. Tuchilus, M. Florescu, Pyridazine and phthalazine derivatives with potential antimicrobial activity, J. Heterocycl. Chem. 44 (2007) 1149–1152.

[22] R.J. Gleave, P.J. Beswick, A.J. Brown, G.M.P. Giblin, P. Goldsmith, C.P. Haslam, W.L. Mitchell, N..H. Nicholson, L.W. Page, S. Patel, S. Roomans, B.P. Slingsby, M.E. Swarbrick, Synthesis and evaluation of 3-amino-6-aryl-pyridazines as selective CB2 agonists for the treatment of inflammatory pain, Bioorg. Med. Chem. Lett. 20 (2010) 465–468.

[23] A.S.A. Youssef, M..I. Marzouk, H.M..F. Madkour, A..M.A. El-Soll, M.A. El-Hashash, Synthesis of some heterocyclic systems of anticipated biological activities via 6-aryl-4-pyrazol-1-yl-pyridazin-3-one, Can. J. Chem. 83 (2005) 251–259.

[24] E..M. Flefel, W.A. Tantawy, W.I. El-Sofany, M. El-Shahat, A.A. El-Sayed, D..N. Abd-Elshafy, Synthesis of some new pyridazine derivatives for anti-HAV evaluation, Molecules 22 (2017) 148.

[25] M. Asif, D. Singh, A. Singh, Analgesic activity of some 6-phenyl-4-substituted benzylidene tetrahydro pyridazin-3 (2H)-ones, Glob. J. Pharmacol. 5 (2011) 18–22.

[26] I.G. Rathish, K. Javed, S. Bano, S. Ahmed, M.S. Alam, K.K. Pillai, Synthesis and blood glucose lowering effect of novel pyridazinone substituted benzenesulfonylurea derivatives, Eur. J. Med. Chem. 44 (2009) 2673–2678.

[27] A..A. Abu-Hashem, U. Fathy, M.A. Gouda, Synthesis of 1, 2, 4-triazolopyridazines, isoxazolofuropyridazines, and tetrazolopyridazines as antimicrobial agents, J. Heterocycl. Chem. 57 (2020) 3461–3474.

[28] J.M. Contreras, Y.M. Rival, S. Chayer, J.J. Bourguignon, C.G. Wermuth, Aminopyridazines as acetylcholinesterase inhibitors, J. Med. Chem. 42 (1999) 730–741.

[29] S. Imad, S. Nisar, Z.T. Maqsood, A study of redox properties of hydralazine hydrochloride, an antihypertensive drug, J. Saudi Chem. Soc. 14 (2010) 241–245.

[30] M. Fung, A. Thornton, K. Mybeck, J.H.H. Wu, K. Hornbuckle, E. Muniz, Evaluation of the characteristics of safety withdrawal of prescription drugs from worldwide pharmaceutical markets-1960 to 1999, Drug Inf. J. 35 (2001) 293–317.

[31] H.H. Sallam, Y.H.E. Mohammed, F.H. Al-Ostoot, M.A. Sridhar, S.A. Khanum, Synthesis, structure analysis, DFT calculations, Hirshfeld surface studies, and energy frameworks of 6-Chloro-3-[(4-chloro-3-methylphenoxy) methyl][1,2,4] triazolo[4, 3-b]pyridazine, J. Mol. Struct. 1237 (2021) 130282.

[32] F.H. Al-Ostoot, D.V. Geetha, Y.H..E. Mohammed, P. Akhileshwari, M.A. Sridhar, S.A. Khanum, Design-based synthesis, molecular docking analysis of an anti-inflammatory drug, and geometrical optimization and interaction energy studies of an indole acetamide derivative, J. Mol. Struct. 1202 (2020) 127244.

[33] G. Sharma, S. Anthal, D.V. Geetha, F.H. Al-Ostoot, Y.H.E. Mohammed, S..A. Khanum, M.A. Sridhar, R. Kant, Synthesis, structure and molecular docking analysis of an anticancer drug of N-(2-aminophenyl)-2-(2-isopropylphenoxy) acetamide, Mol. Cryst. Liq. Cryst. 675 (2018) 85–95.

[34] Z. Zabiulla, V.H. Malojirao, Y.H..E. Mohammed, P. Thirusangu, B..T. Prabhakar, S.A. Khanum, Synthesis, molecular docking, and apoptogenic efficacy of novel N-heterocycle analogs to target B-cell lymphoma 2/X-linked inhibitors of apoptosis proteins to regress melanoma, Med. Chem. Res. 28 (2019) 1132–1160.

[35] L. Krause, R. Herbst-Irmer, G.M. Sheldrick, D. Stalke, Comparison of silver and molybdenum microfocus X-ray sources for single-crystal structure determination, J. Appl. Crystallogr. 48 (2015) 3–10.

[36] A..P.E.X. Bruker, SAINT-plus and SADABS, Bruker AXS Inc., Madison (2004).

[37] G.M. Sheldrick, Crystal structure refinement with SHELXL, Acta Crystallographica Sect. C 71 (2015) 3–8.

[38] A.L. Spek, Single-crystal structure validation with the program PLATON, J. Appl. Crystallogr. 36 (2003) 7–13.

[39] C.F. Macrae, I.J. Bruno, J.A. Chisholm, P.R. Edgington, P. McCabe, E. Pidcock, L. Rodriguez-Monge, R. Taylor, J. van de Streek, P.A. Wood, Mercury CSD 2.0–new features for the visualization and investigation of crystal structures, J. Appl. Crystallogr. 41 (2008) 466–470.

[40] Jr. M.J. Frisch, G.W. Trucks, H.B. Schlegel, G..E. Scuseria, M.A. Robb, J.R. Cheeseman, G. Scalmani, V. Barone, B. Mennucci, G.A. Petersson, H. Nakatsuji, M. Caricato, X. Li, H.P. Hratchian, A.F. Izmaylov, J. Bloino, G. Zheng, J..L. Sonnenberg, M. Hada, M. Ehara, K. Toyota, R. Fukuda, J. Hasegawa, M. Ishida, T. Nakajima, Y. Honda, O. Kitao, H. Nakai, T. Vreven, J.A. Montgomery, J.E. Peralta, F. Ogliaro, M. Bearpark, J.J. Heyd, E. Brothers, K.N. Kudin, V.N. Staroverov, R. Kobayashi, J. Normand, K. Raghavachari, A. Rendell, J.C. Burant, S.S. Iyengar, J. Tomasi, M. Cossi, N. Rega, J.M. Millam, M. Klene, J.E. Knox, J.B. Cross, V. Bakken, C. Adamo, J. Jaramillo, R. Gomperts, R..E. Stratmann, O. Yazyev, A.J. Austin, R. Cammi, C. Pomelli, J.W. Ochterski, R.L. Martin, K. Morokuma, V.G. Zakrzewski, G.A. Voth, P. Salvador, J.J. Dannenberg, S. Dapprich, A.D. Daniels, O. Farkas, J.B. Foresman, J.V. Ortiz, J. Cioslowski, D.J. Fox, Revision A.02, Gaussian Inc. (2009).

[41] M.A. Spackman, D. Jayatilaka, Hirshfeld surface analysis, Cryst. Eng. Commun. 11 (2009) 19–32.

[42] J..I. Aihara, Weighted HOMO-LUMO energy separation as an index of kinetic stability for fullerenes, Theor. Chem. Acc. 102 (1999) 134–138.

[43] R..G. Pearson, Chemical hardness and density functional theory, J. Chem. Sci. 117 (2005) 369–377.

[44] A. Barakat, A.M. Al-Majid, S.M. Soliman, Y.N. Mabkhot, M. Ali, H.A. Ghabbour, H.K. Fun, A. Wadood, Structural and spectral investigations of the recently synthesized chalcone (E)-3-mesityl-1-(naphthalen-2-yl) prop-2-en-1-one, a potential chemotherapeutic agent, Chem. Cent. J. 9 (2015) 1–15.

[45] S.K. Seth, N.C. Saha, S. Ghosh, Structural elucidation and electronic properties of two pyrazole derivatives: a combined X-ray, Hirshfeld surface analyses and quantum mechanical study, Chem. Phys. Lett. 506 (2011) 309–314.

[46] T. Maity, H. Mandal, A. Bauza, B.C. Samanta, A. Frontera, S.K. Seth, Quantifying conventional C-H... π (aryl) and unconventional C-H...π (chelate) interactions in dinuclear Cu (II) complexes: experimental observations, Hirshfeld surface and theoretical DFT study, New J. Chem. 42 (2018) 10202–10213.

[47] J.J. McKinnon, D. Jayatilaka, M..A. Spackman, Towards quantitative analysis of intermolecular interactions with Hirshfeld surfaces, Chem. Commun. 37 (2007) 3814–3816.

[48] S.K. Seth, Structural characterization and Hirshfeld surface analysis of a CoII complex with imidazo [1, 2-a] pyridine, Acta Crystallographica Sect. E 74 (2018) 600–606.

[49] A.J. Edwards, C.F. Mackenzie, P.R. Spackman, D. Jayatilaka, M.A. Spackman, Intermolecular interactions in molecular crystals: what's in a name? Faraday Discuss. 203 (2017) 93–112.

[50] C.F. Mackenzie, P.R. Spackman, D. Jayatilaka, M.A. Spackman, CrystalExplorer model energies and energy frameworks: extension to metal coordination compounds, organic salts, solvates and open-shell systems, Int. Union Crystallogr. J. 4 (2017) 575–587.

[51] M.J. Turner, S..P. Thomas, M.W. Shi, D. Jayatilaka, M.A. Spackman, Energy frameworks: insights into interaction anisotropy and the mechanical properties of molecular crystals, Chem. Commun. 51 (2015) 3735–3738.